

Multiphase flow in porous rock imaged under dynamic flow conditions with fast x-ray computed microtomography

S. Berg^{1,*}, R. Armstrong¹, H. Ott¹, A. Georgiadis¹, S. A. Klapp¹, A. Schwing¹, R. Neiteler¹, N. Brussee¹, A. Makurat¹, L. Leu^{2,1}, F. Enzmann², J.-O. Schwarz², M. Wolf², F. Khan², M. Kersten², S. Irvine³, M. Stampanoni³

¹Shell Global Solutions International BV, The Netherlands.

²Geosciences Institute, Johannes-Gutenberg University, 55099 Mainz, Germany

³Swiss Light Source, Paul Scherrer Institut, 5232 Villigen PSI, Switzerland

This paper was prepared for presentation at the International Symposium of the Society of Core Analysts held in Napa Valley, California, USA, 16-19 September, 2013

ABSTRACT

Pore-scale events in multiphase flow in porous rock have been directly imaged in real-time by using fast synchrotron-based x-ray computed microtomography. In the past, pore-scale fluid displacements in porous media could only be imaged under quasi-static conditions where at scanning times of several minutes to hours, fluid distributions were subject to capillary re-distribution. Here, pore-scale displacement events in porous rock were imaged *in situ* in real-time in natural rock under dynamic flow conditions, where the pressure gradient and the visco-capillary balance were maintained during scanning. Two elementary processes, Haines jumps in drainage and snap-off in imbibition, were studied in detail for sintered glass, sandstone, and carbonate rock. We found that most Haines jump events do not displace the wetting phase pore-by-pore, but typically involve 10-20 individual pores and that filling events are cooperative. We also found that in sandstone rock 64% of the externally applied work is actually dissipated during these jumps where approximately 36% is converted into interfacial energy.

INTRODUCTION

Many aspects of multiphase flow in porous rock are still not very well understood. Commonly used approaches to describe macroscopic fluid behavior are phenomenological, have many shortcomings [1] and lack a consistent link to elementary pore-scale displacement processes like the filling of pores in drainage (Haines jumps [2]) and the disconnection of the non-wetting phase (snap-off [3]). Since porous rock is optically opaque, previous understandings have been developed from studying model materials like 2D glass micromodels which suggest that the transport of the non-wetting (oil) phase is mainly characterized by a repeated break-up and coalescence of disconnected ganglia [4]. This break-up and coalescence is seen to be ultimately the cause of many macroscopic effects like hysteresis, trapping, residual oil, the rate dependency of relative permeability, and dynamic effects in capillary pressure [4]. The question is now to which extent these observations obtained in 2D micromodels apply

also to 3D rock since many of the very elementary displacements have never been directly imaged in real rock which is substantially more complex and differs from 2D micromodels in many relevant characteristics (e.g. coordination number, percolation threshold, mineralogy and etc.). Therefore, the first step is to actually image the displacements at the pore-scale at real-time. Herein, pore-scale 2-phase flow displacements in sintered glass, sandstone, and carbonate rock were imaged under dynamic flow conditions. This was achieved by fast synchrotron-based x-ray computed microtomography [6-10] (μ CT) with scanning intervals of 16.8–42 s for a full tomogram, which is sufficiently fast to capture the capillary equilibrium in-between the few millisecond lasting Haines jumps [10]. While studies in the past conducted at longer scanning times could only address quasi-static situations where flow had been stopped, the scanning interval of seconds and an *in-situ* micro-pump integrated into the flow cell allowed for the study of individual pore drainage events (Haines jumps [2]) and snap-off [3] events in imbibition under dynamic flow conditions (i.e. by maintaining flow and pressure gradients [10]).

METHODS AND MATERIALS

The approach is conceptually similar to rate-controlled Hg-air porosimetry APEX [11,12] but thanks to more sensitive modern pressure sensors (Keller 2 Mi), oil-water systems are studied, and the *in-situ* fluid configuration is imaged with fast μ CT.

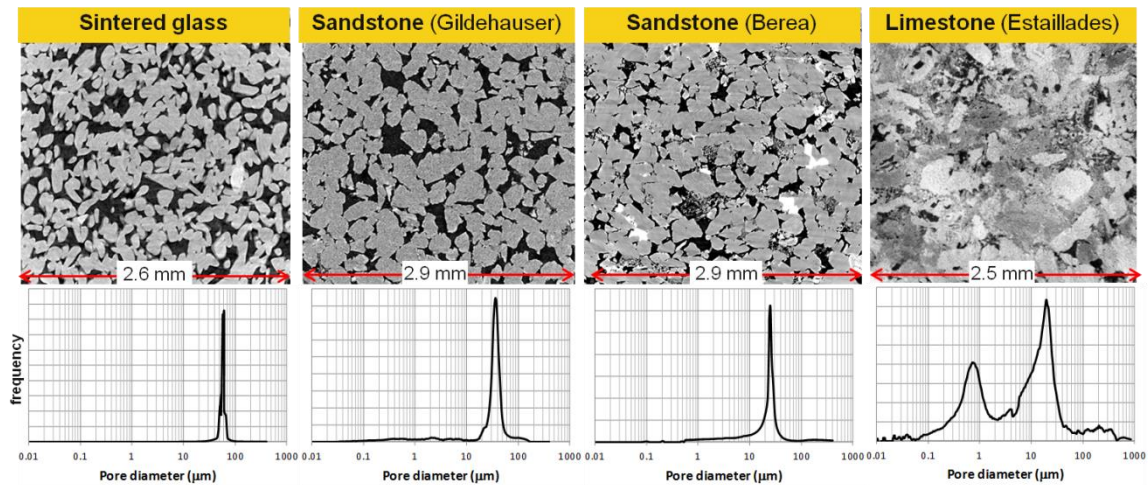


Figure 1: μ CT scans (top row), pore size distribution (Hg-air) of sintered glass, sandstone rock and limestone (bottom row).

Cylindrical samples (4 mm diameter and 10 mm length) of sintered glass (Robuglass, ($\phi=31.8\%$, $K=22\pm 2$ D [13,14]), Gildehauser (Bentheimer type, $\phi=23.8\%$, $K=1.5\pm 0.3$ D), Berea sandstone ($\phi=19.9\%$, $K=700$ mD), and Estailades limestone ($\phi=28.4\%$, $K=200\pm 60$ mD) - μ CT slices are displayed in Figure 1 - were embedded into

polycarbonate by heat-shrinking. The assembly was mounted on a sample holder with an integrated micro-piston pump (the setup is displayed in Figure 2) which prevents displacement artifacts caused by the bending of external flow lines during stage rotation during x-ray tomography or when opening and closing the valves.

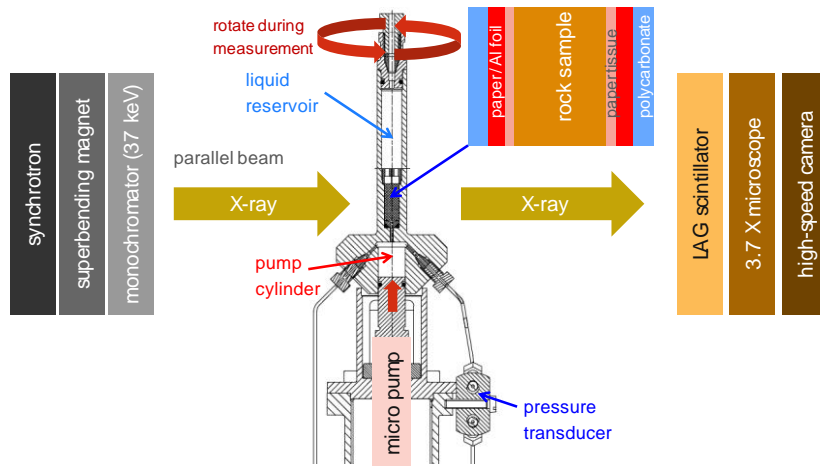


Figure 2: Experimental setup with sample holder in synchrotron beamline. Large photon flux, a high-speed camera and an *in-situ* micro-pump allows for dynamic measurements under flow conditions. The rock sample is wrapped in paper tissue to prevent artificial fluid distributions (i.e. oil phase flowing along oil-wet polycarbonate wall).

The x-ray tomography experiments were performed at the TOMCAT beamline at the Swiss Light Source [9]. The transmitted x-rays were converted into visible light by a 100 μm -thick cerium-doped lutetium aluminum garnet (LAG) scintillator and $3.7 \times$ optically magnified. The Berea sandstone sample (2011 data) was imaged at an x-ray energy of 21.25 keV and using a PCO.Dimax high-speed camera (12 bit CMOS, resolution 2.99 $\mu\text{m}/\text{pixel}$) at a time resolution of 16.8 s. The internal camera memory of 32 GB allowed for the capture of 7 full tomograms followed by a subsequent data readout time of ~ 15 minutes. The other samples were studied in 2012 using a PCO.edge camera (16 bit sCMOS, resolution 2.2 $\mu\text{m}/\text{pixel}$), which allows continuous read-out at a time resolution of 20-60 s. The x-ray energy used was 37 keV which is directly above the K-edge of cesium which was used as a contrast agent for the phase water. In the Berea experiments, oil (n-decane) is injected from the feed pump upwards into the sample at a capillary number ($\text{Ca} = \mu v / \sigma$ with velocity v , viscosity μ and interfacial tension σ) of 4×10^{-8} . For the other samples, the flow direction was reversed for easier handling, at $\text{Ca} = 4 \times 10^{-9}$ to be able to increase the scanning time/intervals.

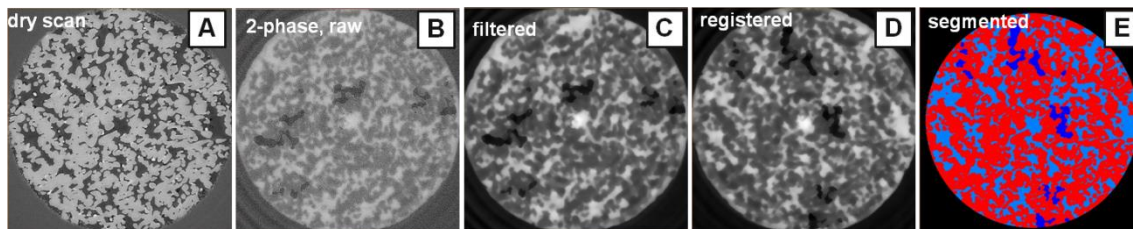


Figure 3: Image processing workflow - segment dry scan (A), 2-phase raw data (B) filtered by non-local means (C), registration to dry scan (D) and global segmentation by watershed of oil (E).

The image processing workflow is sketched in Figure 3 for the sintered glass data. Initially, the data is filtered then the flow experiment scans are registered to a dry scan to mask the pore-space and lastly the images are segmented using a watershed-based segmentation routine (Avizo fire, Visualization Sciences Group).

RESULTS

Primary drainage in sintered glass

In Figure 4, a time sequence during primary drainage (i.e. decane invades the water saturated sintered glass sample) is displayed.

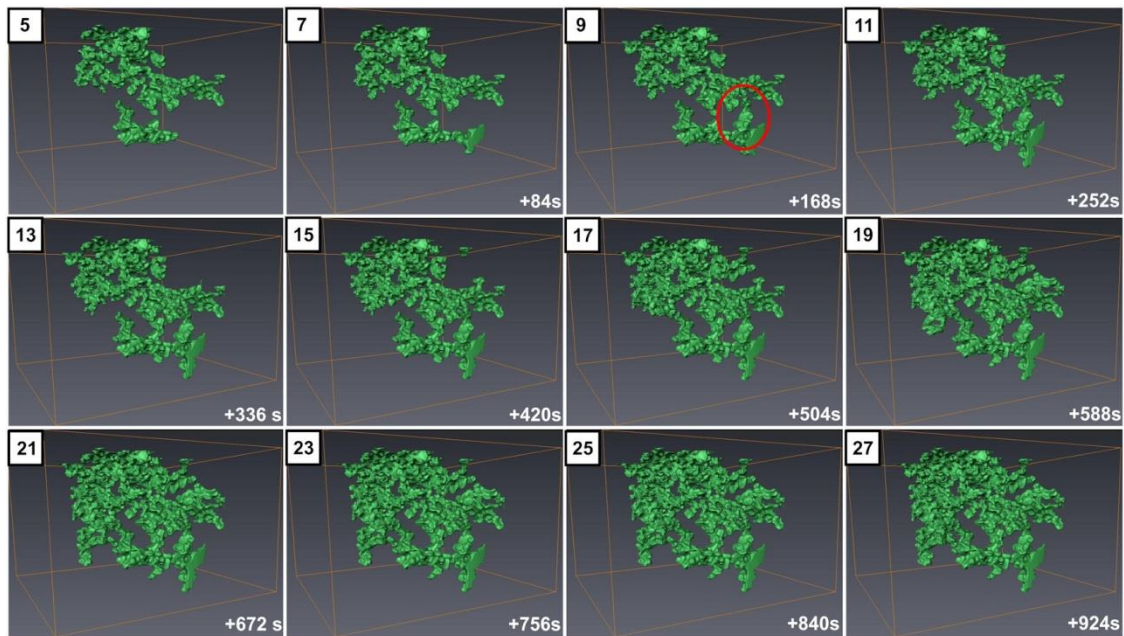


Figure 4: Image sequence during primary drainage of decane (green) into sintered glass at $Ca=4\times 10^{-9}$. For better visibility, here only every 2nd scan is shown.

Figure 4 illustrates that pore drainage is not caused by continuous flow but by step-wise invasion of decane. That is also reflected by the observed spikes in the pressure data (referred to as a "rheon" [15,11]) displayed in Figure 5 which are indicative of a Haines jump (note that pressure signal for this sample is inverted compared to traditional APEX because it was operated in suction). As shown in Figure 5, these pressure spikes correspond well with the pore drainage event observed in the μ CT data.

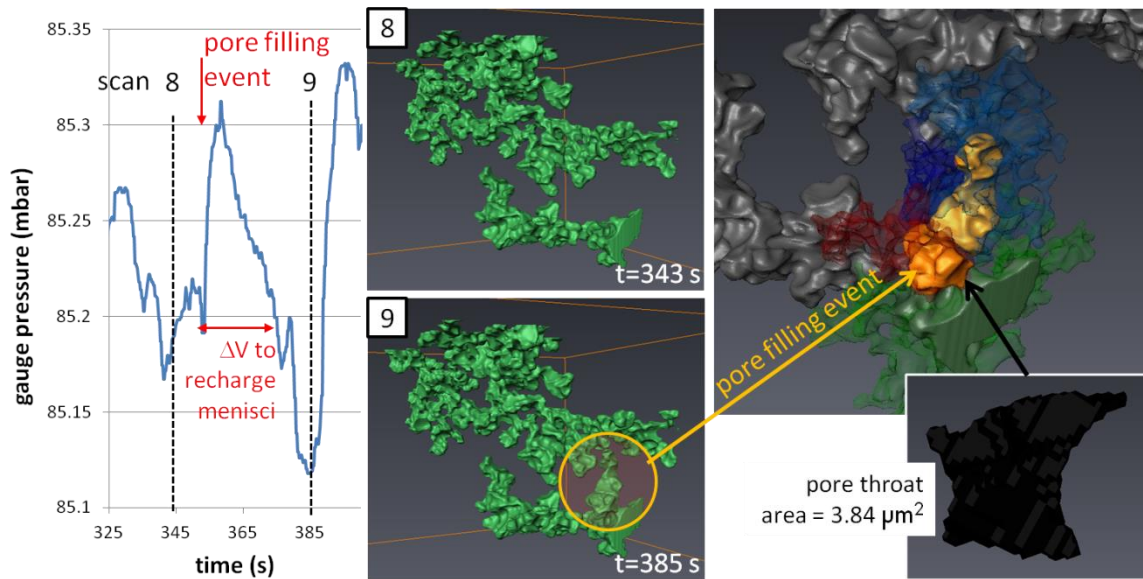


Figure 5: Pore drainage event observed in the pressure signal corresponds well with the μ CT data.

Primary drainage in Berea sandstone

In Figure 6, an image sequence is displayed wherein decane is invading the pore space of a water saturated Berea sandstone rock.

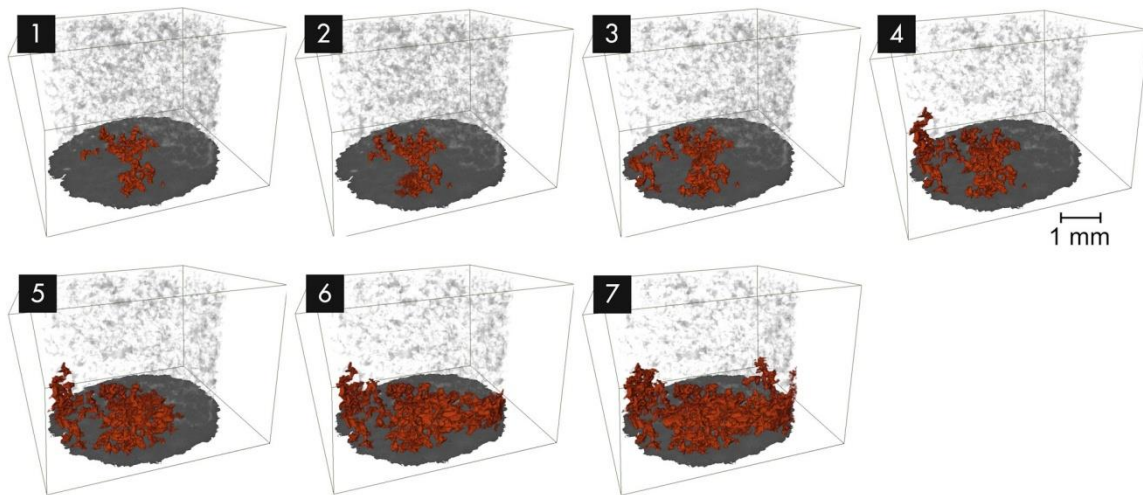


Figure 6: Image sequence showing the invasion of decane (red) into a water saturated Berea sandstone (semi-transparent grey) in primary drainage at a flow rate of $1.54 \mu\text{m/s}$ (0.4 ft/d , corresponding to a capillary number, $\text{Ca}=4 \times 10^{-8}$). Time difference between individual images is 16.8 s .

A more detailed view, in a small region of interest, is displayed in Figure 7 which shows the process of pore drainage in more detail. We observe events where single large pores are drained but also where whole systems of pores are drained in cascade-like events.

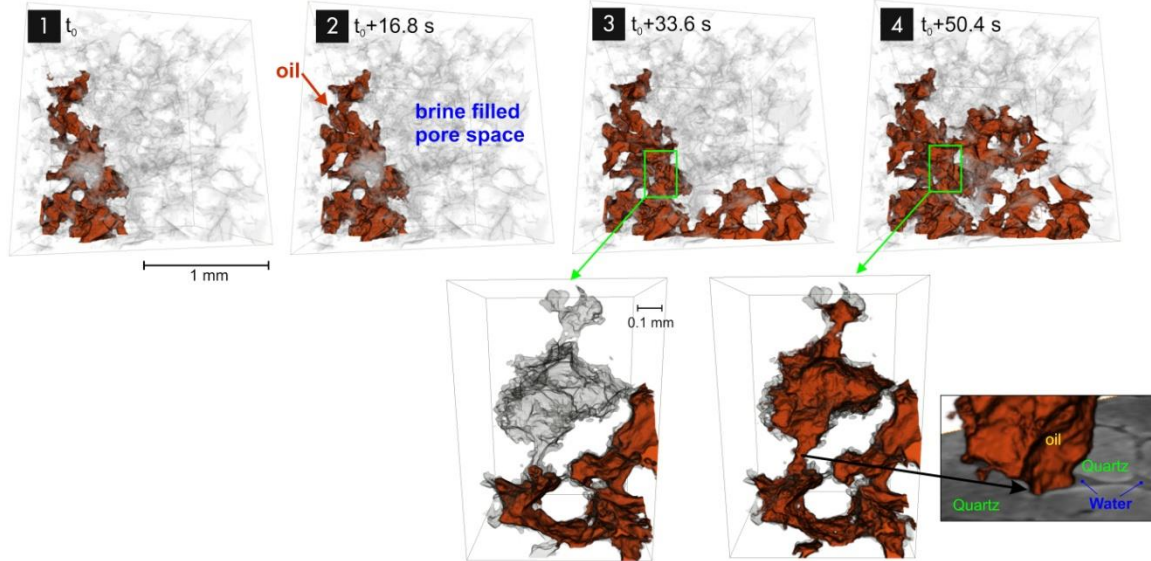


Figure 7: Region of interest from Figure 6. The close-up in the bottom panel shows the drainage of a single individual pore. A cross section through the pore throat shows that the non-wetting phase is located in the center surrounded by the wetting phase (bottom right).

The pressure data for the drainage sequence from Figure 6 and displayed in Figure 8 clearly shows that pore drainage events occur every 10-20 s during drainage (at $Ca=4 \times 10^{-8}$) which means that a scan interval of 15-60 s is fast enough to capture fluid configurations between the individual Haines jumps. The pressure data shows that individual events range up to 100-200 nL (consistent with the μ CT data), whereas the pore size distribution indicates that the largest pores by geometrical definition are only 1-10 nL. Pressure and imaging data clearly show that pores are not drained one-by-one but in cascading events draining multiple geometrically defined pores in one step [15]. At typical field flow rates, drainage events repeat every 10-20 s in the tested rock sample whereas the actual Haines jump lasts only 1-10 ms [16,17] which is equivalent to the exposure time for a single radiograph and thus is far too fast for volume data (i.e. μ CT). The time scale for pore drainage (~milliseconds) is interesting in another respect. For example, a pore of 5.9 nL volume as in the bottom panel of Figure 7 drained in 1-10 ms which implies an effective drainage rate of 5900 nL/s which exceeds 100-1000 times the rate of the feed pump (5.8 nL/s). This means that pores are actually not drained by the feed pump or a large-scale flow field but are rather a local re-arrangement of non-wetting fluid, for instance fluid "stored" in liquid-liquid menisci and/or pore necks in adjacent regions. Overall, these results suggest the pore drainage occurs as cooperative events, which has been postulated [15] and inferred from indirect data [13] before, but for which now direct evidence is provided.

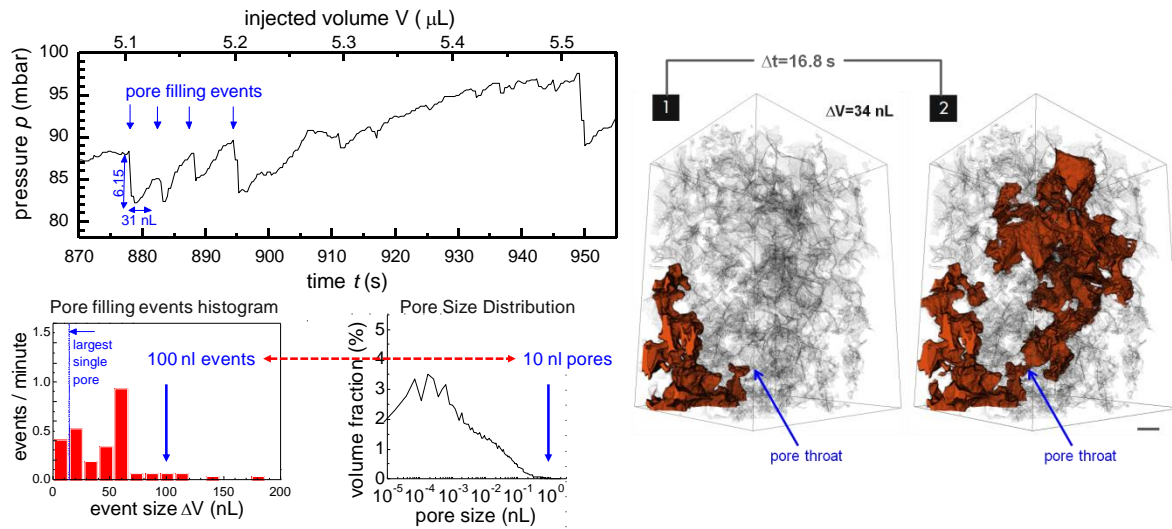


Figure 8: Left panel: The pressure in the oil phase shows discrete jumps representing pore drainage events (Haines jumps). The magnitude of the events ranges up to 100-200 nL (event size histogram, bottom left) which is about 10-100 times larger than the largest individual pore (pore size distribution). Instead of individual pores being drained one-by-one, entire pore systems consisting of multiple pores, are drained in one step (see example in the right panel).

To directly visualize this cooperative behavior we conducted experiments in 2D micromodels imaged at 2000 frames/s [18] which captures the transient dynamics during a Haines jumps. In Figure 9, we show an example of a pore drainage event in a system of 60 μm diameter pores with 13 μm wide pore throats (at 5 μm depth).

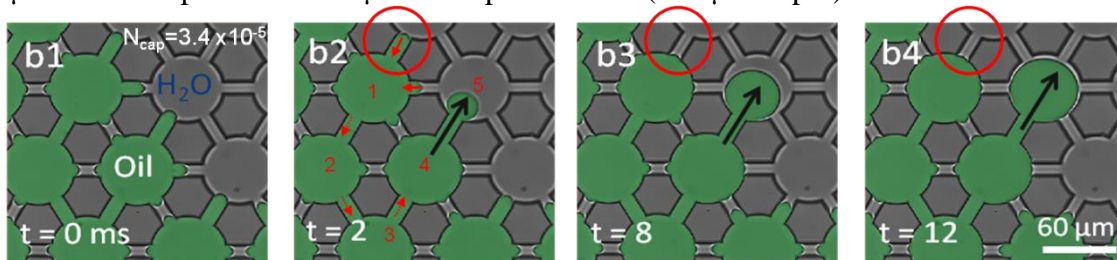


Figure 9: Cooperative pore drainage events a 2D glass micromodel imaged with a high speed camera.

Drainage of pores (black arrow) leads to retraction of the nearby menisci (red circles).

When a pore body is drained, retraction of nearby menisci occurs which supplies the volume of fluid required for the drainage event. The drainage is driven by the difference in capillary pressure at the front (wide pore = small curvature) and the nearly constantly high capillary pressure in the meniscus. During this process the elastic energy initially stored in the meniscus is converted into kinetic energy [16] which is largely dissipated by viscous forces until a new capillary equilibrium is reached and fluid is temporarily static. In this way, the pore scale flow can be categorized into rapid (only few millisecond lasting), irreversible events (Haines jump, "rheon") [15] and much slower (few seconds lasting) laminar flow phases where the menisci are re-charged to the same curvature/pressure before the Haines jump ("subison") and further increased ("rison")

[11] until the pore entry pressure of the next pore system is exceeded and another Haines jump occurs. This division into subisons and risons allows for estimating the pressure-volume work ($W = \int p dV$) dissipated during a Haines jumps. From the pressure data, for the case of Berea sandstone (Figure 8), we estimate that 39% of the displaced volume occurs through reversible drainage of pore throats (rison events) and 61% occurs via rapid irreversible events which dissipate 64% of the total work of drainage which is consistent with previous reports on Berea sandstone [19]. During a pore drainage event, the energy is not completely dissipated but in part converted into interfacial energy as expressed in a pore scale energy balance [15]

$$\Delta F = -S\Delta T + \sum_{\alpha=1}^2 p_{\alpha} \Delta V_{\alpha} + \sigma_{12} \Delta A_{12} \quad (1)$$

While the pressure-volume work term $p\Delta V$ is accessible through pressure data like in Figure 8 and the interfacial energy term $\sigma\Delta A$ term (σ_{12} is the interfacial tension and A_{12} the oil-water interfacial area) is only accessible through μ CT data. For the event of the single big pore from the bottom panel of Figure 7, the interfacial area, including the area in which thin water films separate oil and water-wet rock, is $\Delta A_{1,2} = 5.7 \times 10^{-7} \text{ m}^2$. At a water-decane interfacial tension of $\sigma_{12} = 35 \text{ mN/m}$, this corresponds to an interfacial energy of 36% of the displacement pressure-volume work (i.e. $p\Delta V$).

Drainage in limestone

In addition to the sintered glass and sandstone samples, drainage in Estailades limestone sample was also studied. An example of the drainage sequence is displayed in Figure 10.

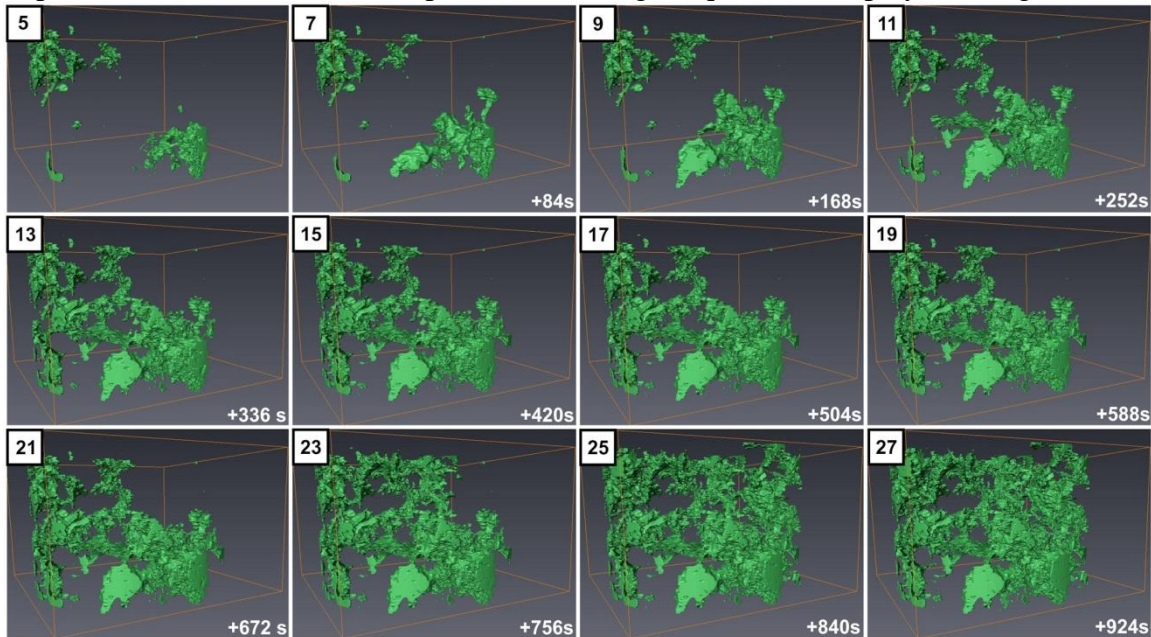


Figure 10: Image sequence during drainage in Estailades limestone.

In primary drainage, initially the large connected macro-pores are filled which is displayed in the sequence in Figure 10. In comparison to the sintered glass and sandstone experiments, the largest pore filling events (Figure 11) are bigger beyond what can be explained directly from differences in the pore size distribution (see Figure 1), i.e. the large events are a factor of 10-50 bigger than the biggest pores.

Filling Event Statistics

In Figure 11, the event size distribution N for the drainage events in the sintered glass (Figure 4), Gildehauser, and Estailades (Figure 10) samples are displayed as a function of the event volume ΔV normalized to the volume of the average pore V_{pore} .

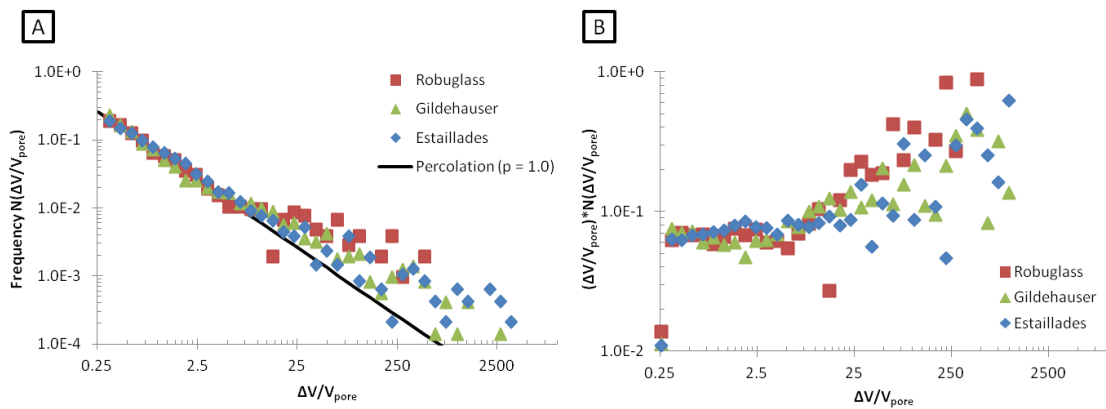


Figure 11: Drainage event size distribution: (A) frequency $N(\Delta V/V_{\text{pore}})$ and (B) displacement volume-weighted distribution $\Delta V/V_{\text{pore}} * N(\Delta V/V_{\text{pore}})$ as a function of event volume ΔV normalized to the volume of the average pore V_{pore} . For small events sizes $\Delta V/V_{\text{pore}}$ the distribution N follows an power law $N \sim (\Delta V/V_{\text{pore}})^{-1.0}$ (black line) but larger events (which mainly contribute to saturation, see B) are more frequent than predicted by percolation.

Event sizes range over almost 4 decades which is significantly broader than the pore size distributions of at least the sintered glass and sandstone samples (Figure 1). This suggests that the event size distribution is not directly related to the pore size distribution. For small events ($\Delta V/V_{\text{pore}}$), the event size distribution in Figure 11A follows an invasion-percolation power law behavior as reported in simulations and micromodel experiments by [20]

$$N(\Delta V / V_{\text{pore}}) \propto (\Delta V / V_{\text{pore}})^{-p} \quad (2)$$

However, we measure $p=1.0$ whereas in micromodel experiments exponents of 1.527 and 1.9 are reported [20]. Additionally, in real rock we find large events that are more frequent than predicted by invasion percolation theory (see Figure 11A, $\Delta V/V_{\text{pore}} > 25$). It is particularly these large events that significantly contribute to saturation as the volume-weighted distribution in Figure 11B demonstrates, i.e. this may be a very relevant effect and requires further investigation in more detail.

Imbibition and Capillary De-Saturation

In addition to drainage, imbibition was also studied. In Figure 12, we show an example of a snap-off [3,21] event in Berea sandstone which leads to disconnection of the oil phase and ultimately capillary trapping.

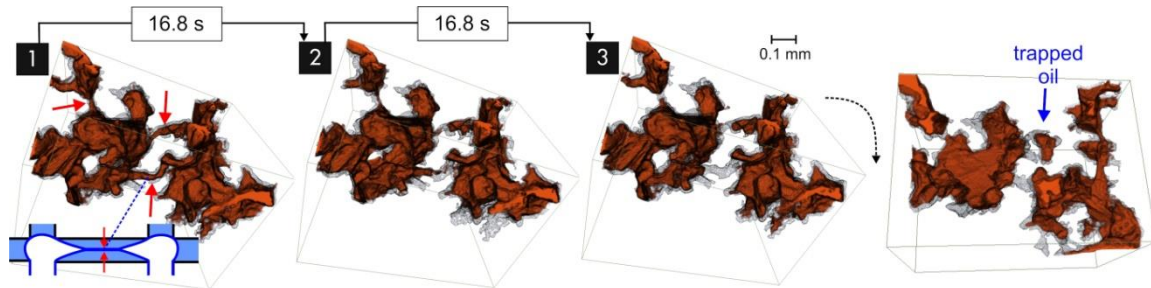


Figure 12: Snap-off (red arrows) during imbibition leading to trapping of oil (blue arrow)

After capillary trapping, as flow rate is increased, oil saturation is systematically decreased. This behavior is typically observed for capillary de-saturation [5] and was also observed in our experiments (see Figure 13 and 14A for the sintered glass sample).

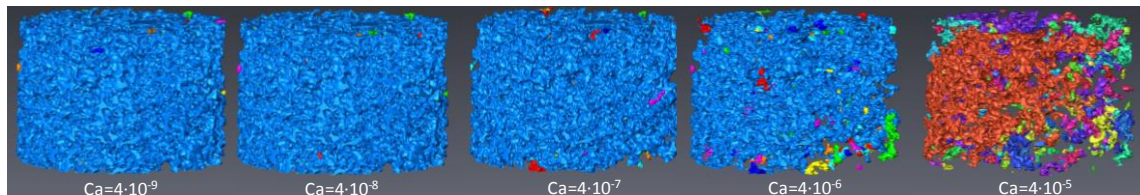


Figure 13: Capillary de-saturation [5] in sintered glass. As the flow rate is increased the oil phase disconnects and the number of clusters increases (color coding indicates connectivity).

We observe the typical behavior of capillary de-saturation [5] where the remaining oil saturation remains nearly constant ("plateau" [5]) below a critical capillary number (which is here around $Ca \sim 3 \cdot 10^{-8}$ for the sintered glass sample) and then decreases when the capillary number is further increased (Figure 14A). Below the critical capillary number the viscous forces (i.e. the viscous pressure drop over the clusters) are not sufficient to overcome the trapping capillary forces and hence even the largest oil cluster remains constant (Figure 14B). When Ca is increased above this threshold, the largest cluster cannot withstand the mobilizing viscous pressure drop and is therefore mobilized and/or breaks apart by snap-off (like in Figure 12) into smaller clusters, for which the data in Figure 14 provides direct evidence: the largest cluster decreases and the second largest cluster increases (Figure 14). Upon further increase of Ca the number of disconnected oil clusters is increasing. Note that in comparison to most capillary de-saturation studies on larger cores reported in the literature, here the starting point is an initial water saturation of 25% obtained at the end of the drainage cycle which is larger

than the true connate water saturation (which is expected around 5-10% in sintered glass) and that after the first water flood (i.e. lowest Ca) the remaining oil saturation is still 75% which could be caused by a capillary end-effect in our short samples.

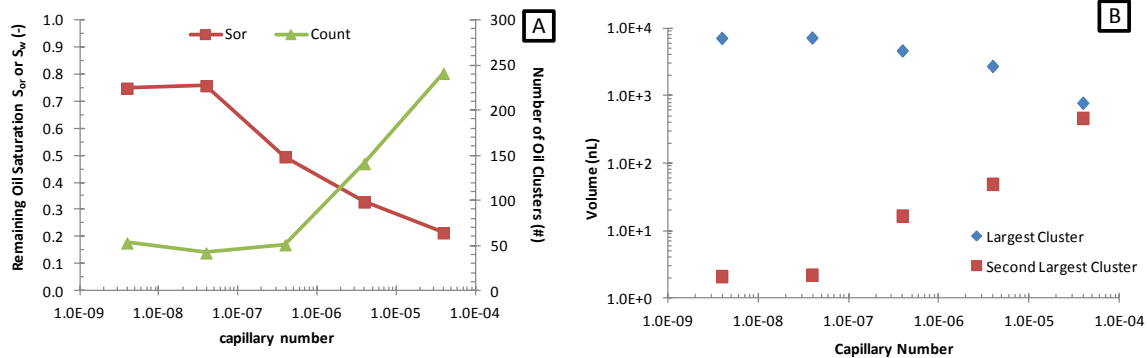


Figure 14: During capillary de-saturation, as the flow rate is increased the oil phase saturation is decreased which leads to an overall increase of disconnected oil clusters (A). The largest cluster decreases in size and the second largest cluster increases (B).

CONCLUSIONS

Real-time imaging of pore scale events in multiphase flow under dynamic flow conditions has been demonstrated using fast synchrotron-based x-ray computed microtomography. Developments over the past years have matured this technology to a level where it can be used to monitor pore scale processes during flow experiments to gain new fundamental insights. We found that most Haines jump events do not displace the wetting phase pore-by-pore, but typically involve 10-20 individual pores and that drainage events are cooperative (i.e. interacting with fluid menisci in adjacent pores). We also found that in sandstone rock 64% of the externally applied work is actually dissipated during these jumps where approximately 36% is converted into interfacial energy. During imbibition, snap-off events were directly observed. In a capillary de-saturation experiment, at increased flow rates an initially large non-wetting phase cluster breaks apart into smaller individual clusters. In addition, the resulting data sets can serve as reference data to directly validate digital rock technology [22] on the basis of displacement data [23].

Lastly, the distribution of pore drainage events agrees with invasion-percolation theory only for small events. However, the large events which significantly contribute to saturation occur more frequently than predicted by invasion-percolation.

ACKNOWLEDGMENTS

F. Marcelis and A. Coorn are acknowledged providing the 4 mm diameter rock samples; H. van der Linde for conducting the interfacial tension measurements; T. Blok and J. Hofman for the MICP measurements. We thank C. van Kruijsdijk for helpful discussions

on the energy dissipation section. μ -CT was performed at the TOMCAT beamline at the Swiss Light Source, Paul Scherrer Institut, Villigen, Switzerland. We are grateful to G. Mikuljan at the Swiss Light Source for his contribution to these experiments.

REFERENCES

- * Corresponding author; E-mail address: steffen.berg@shell.com
1. J. Niessner, S. Berg, S. M. Hassanizadeh, Comparison of Two-Phase Darcy's Law with a Thermodynamically Consistent Approach, *Transport in Porous Media* 88:133–148, 2011.
 2. W. B. Haines, Studies in the physical properties of soils. V. The hysteresis effect in capillary properties, and the modes of water distribution associated therewith. *J Agric Sci* 20(1):97–116, 1930
 3. J. G. Roof, Snap-off of oil droplets in water-wet pores. *SPE J* 10(1):85–90, 1970.
 4. D. G. Avraam and A. C. Payatakes, Flow regimes and relative permeabilities during steady-state two phase flow in porous media, *Journal of Fluid Mechanics* 293, 207-236, 1995.
 5. L. W. Lake, *Enhanced Oil Recovery*, Prentice Hall, 1989.
 6. S. Iglauer, A. Paluszny, C. Pentland, and M. Blunt, (2011) Residual CO₂ imaged with X-ray micro-tomography. *Geophys Res Lett* 38(21):L21403.
 7. D. Wildenschild, et al. (2002) Using x-ray computed tomography in hydrology: Systems, resolutions, and limitations. *J Hydrol (Amst)* 267:285–297.
 8. S. Youssef, M. Han, D. Bauer, E. Rosenberg, S. Bekri, M. Fleury, O. Vizika, "High Resolution μ -CT combined to numerical models to assess electrical properties of bimodal carbonates." in 22nd International Symposium of the Society of Core Analysts, Abu Dhabi, UAE, 2008.
 9. R. Mokso, et al. (2011) Following dynamic processes by X-ray tomographic microscopy with sub-second temporal resolution. *AIP Conf Proc* 1365, pp 38–41. Available at <http://dx.doi.org/10.5167/uzh-57653>.
 10. S. Berg *et al.*, Real-time 3D imaging of Haines jumps in porous media flow, *Proceedings of the National Academy of Sciences (PNAS)* 110 (10), 3755–3759 (2013).
 11. H. H. Yuan, B. F. Swanson, Resolving pore-space characteristics by rate-controlled porosimetry. *SPE Form Eval* 4(1):17–24, 1989.
 12. H. H. Yuan, Advances in APEX technology, SCA Conference paper SCA1990-04, 1990.
 13. A. Georgiadis, S. Berg, G. Maitland, and H. Ott, Pore-Scale micro-CT Imaging: Non-Wetting Phase Cluster Size Distribution during Drainage and Imbibition, submitted to *Physical Review E*, 2013.
 14. A. Georgiadis, S. Berg, G. Maitland, and H. Ott, Pore-Scale Micro-CT Imaging: Cluster Size Distribution during Drainage and Imbibition, *Energy Procedia* 23 (2012) 521 – 526
 15. N. R. Morrow, Physics and thermodynamics of capillary action in porous media. *Ind Eng Chem* 63(6):32–56, 1970.
 16. K. K. Mohanty, H. T. Davis, L. E. Scriven, Physics of oil entrapment in water-wet rock. *SPE Res Eval & Eng* 2(1):113–128, 1987.
 17. D. A. DiCarlo, J. I. G. Cidoncha, C. Hickey, Acoustic measurements of pore scale displacements. *Geophys Res Lett* 30(17):1901, 2003.
 18. R. Armstrong, S. Berg, Interfacial velocities and capillary pressure gradients during Haines jumps, in preparation.
 19. S. Seth, N. R. Morrow, Efficiency of the conversion of work of drainage to surface energy for sandstone and carbonate. *SPE Res Eval & Eng* 10(4):338–347, 2007.
 20. D. Crandall, G. Ahmadi, M. Ferer, D. H. Smith, Distribution and occurrence of localized-bursts in two-phase flow through porous media, *Physica A* 388, 574-584, 2009.
 21. R. Lenormand, C. Zarcone, A. Sarr, Mechanisms of the displacement of one fluid by another in a network of capillary ducts. *J Fluid Mech* 135:337–353, 1983.
 22. J. Schembre-McCabe, R. Salazar-Tio, G. Ball and J. Kamath, A Framework to Validate Digital Rock Technology, SCA2011-28.
 23. D. Koroteev et al., Direct Hydrodynamic Simulation of Multiphase Flow in Porous Rock, SCA2013-014.